Journal of Magnetism and Magnetic Materials 423 (2017) 46–50

Contents lists available at ScienceDirect

Journal of Magnetism and Magnetic Materials

journal homepage: www.elsevier.com/locate/jmmm

Elemental moment variation of bcc Fe_xMn_{1-x} on MgO(001)

H. Bhatkar[a], R.J. Snow[a], E. Arenholz[b], Y.U. Idzerda[a,*]

[a] Department of Physics, Montana State University, Bozeman, MT 59717, USA
[b] Advanced Light Source, Lawrence Berkeley National Laboratories, Berkeley, CA 94720, USA

ARTICLE INFO

Keywords:
Bcc FeMn alloy
X-ray absorption spectroscopy
X-ray magnetic circular dichroism
Magnetic thin films

ABSTRACT

We report the growth, structural characterization, and electronic structure evolution of epitaxially grown bcc Fe_xMn_{1-x} on MgO(001). It is observed that the 20 nm thick Fe_xMn_{1-x} alloy films remained bcc from $0.65 \le x \le 1$, much beyond the bulk stability range of $0.88 \le x \le 1$. X-ray absorption spectroscopy and X-ray magnetic circular dichroism show that both the Fe and Mn L_3 binding energies slightly increase with Mn incorporation and that the elemental moment of Fe in the 20 nm crystalline bcc alloy film remain nearly constant, then shows a dramatic collapse near x~0.84. The Mn MCD intensity is found to be small at all compositions that exhibit ferromagnetism

1. Introduction

Thin films of fcc Fe_xMn_{1-x} have been of excitement in the area of magnetic storage for a considerable time due to their application as the alloy of choice in multilayer systems that form magnetoresistance read heads [1]. In terms of the exchange-biasing achieved using the Fe_xMn_{1-x} materials, it was observed that the fcc $Fe_{0.5}Mn_{0.5}$ (x=0.5 or 50% Mn lattice site occupancy – all percentages are lattice site occupations) was stable and antiferromagnetic (AFM) in thin film form at room temperature [2], which became the key motivation to study FeMn in various structures and in thin films. The antiferromagnetic Fe_xMn_{1-x} alloy in fcc phase have been stabilized in the $0.5 \le \times \le 0.7$ range [3] on various substrates such as copper [4]. Crystalline thin films reduce the complexity of the possible magnetic structures allowing for a clearer identification of the magnetic structure associated with the alloy. Since the fcc Fe is AFM [5] and bcc Fe is ferromagnetic (FM) [6], determining the mechanism of the magnetic moment variation in the ferromagnetic phase becomes of interest not only for moment control, but as guidance for applications that take advantage of exchange bias of fcc FeMn layers where the magnitude of the elemental moments at the AF interface plays an important role.

The bulk bcc Fe_xMn_{1-x} alloy is intriguing because of its departure from the Slater-Pauling curve [7,8]. The average moment per atom of nearly all transition metal binary alloys is found to first increase with the electron filling, then decrease above a critical value. For FeMn, the average alloy moment follows this trend only for the high Fe concentrations (see Fig. 1). At x=0.88 (12% Mn lattice site occupancy), the bulk average moment rapidly vanishes, suggesting the onset of a magnetic phase transition. Earlier works reported that the low concentration of Mn are stable in the bcc structure only up to 5% Mn [9], then later revised up to x=0.88 (12% Mn) [10]. In many cases, substrate stabilization have allowed for the stabilization of unfavored structures beyond the bulk limit and have even stabilized crystal structures not found in the bulk [11].

Some binary alloys that seem to deviate from the Slater-Pauling behavior of Fig. 1 are actually in agreement with Friedel's interpretation [12] of the Slater-Pauling behavior. This can be visualized if the magnetic moment per atom is plotted as a function of the average magnetic valence [13] resulting in a straight line, in contrast to the conventionally plotted volcano shaped Slater-Pauling curve [14]. Some alloy systems involving AFM-FM transition metal alloys that are identified as departures in the conventional plot, become regularly behaved points around the central trend-line [13]. Plotting the FeMn data in this manner again shows a marked departure from the anticipated straight line (due to the abrupt loss of magnetization).The reported growth of bcc Fe_xMn_{1-x} films is limited. The structure was first stabilized as 2.5 nm thick films as $Fe_{0.9}Mn_{0.1}$/Ir(001) superlattices [15], then stabilized with a slight tetragonal distortion on GaAs(001) substrates to x=0.8 (20% Mn) for films less than 3 nm thick [16], and subsequently stabilized as ultrathin films (< 6 ML) on Ag(001) to x=0.72 (28% Mn) [17]. Here we report the growth and magnetic moment variation of bcc Fe_xMn_{1-x} single crystal films on MgO(100). Interfaces with MgO are of particular interest for TMR devices [18,19]. Only states that can exist on both sides of the interface of Fe-MgO control the coherent tunneling current in these devices [20]. Such matching of states across the interface is a very sensitive function of parameters like crystallinity and the abruptness of the interface. Mixing of Fe and Mg at the interface can strongly affect the filtering effect

* Corresponding author.
E-mail address: idzerda@montana.edu (Y.U. Idzerda).

http://dx.doi.org/10.1016/j.jmmm.2016.09.060
Received 10 March 2016; Received in revised form 5 July 2016; Accepted 11 September 2016
Available online 13 September 2016
0304-8853/

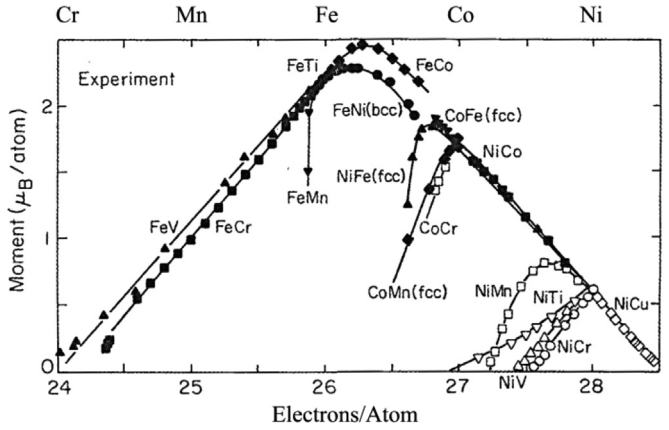

Fig. 1. Slater-Pauling curve of measured bulk atomic moments for different transition metal alloys as a function of electron filling (from Ref. [8]).

across the barrier [21] and has been attributed to reduction of the predicted value of 1500% TMR of Fe/MgO/Fe magnetic tunnel junctions to experimentally achieved one of 180% [19].

2. Experimental details

Using Molecular Beam Epitaxy (MBE), single crystal films of Fe_xMn_{1-x} were deposited on polished single crystal MgO(001) substrates. The MgO substrate cleaning procedure consisted of sonication of the MgO substrate in acetone followed by sonication in methanol for 5 min. Usually, as the third step in the triple-wash technique, substrates are rinsed in de-ionized water, but due to the hygroscopic nature of MgO, this final step was avoided. After flowing dry nitrogen over the freshly sonicated MgO, these substrates were quickly mounted onto a molybdenum holder using indium solder and loaded into high vacuum. The substrates were then heat-treated to clean any possible adsorbed contaminants by annealing in vacuum at 800 °C (1073 K) for 2 min. This cleaning procedure has been shown to produce single crystal epitaxial growth with minimal interfacial oxidation of the Fe [22,23].

The base pressure just prior to growth was ~1.0×10^{-9} Torr and during film growth with all Knudsen Cell sources at their operating temperatures, the pressure raised to ~2.5×10^{-9} Torr. For all growths, the Fe source was always maintained at constant temperature of ~1400 °C (1673 K) assuring a constant rate of Fe deposition while the Mn source was held at various temperatures to achieve different Mn flux rates and therefore different alloy stoichiometries for the films. The films were deposited with the substrate held at 150–160 °C (423–433 K) to ensure good quality, ~20 nm thick films [24]. Deposition fluxes were monitored by quadrupole mass spectrometry (QMS). A layer of amorphous aluminum of thickness 3.5 nm was deposited as a capping layer. Substrates were cooled to 70 °C (343 K) before deposition of Al capping layer to minimize any interlayer mixing between the FeMn film and Al capping layer. Film compositions were verified by comparison of the Fe and Mn integrated L_3-edge XAS intensities and film thicknesses were calibrated by Rutherford Backscattering Spectrometry (RBS).

3. Results and discussion

The bare MgO(001) substrate surface quality was first characterized in ultra-high vacuum using *in-situ* Reflection High Energy Electron Diffraction (RHEED) imaged immediately after heat treatment. Since MgO is an insulating material, substrate charging can distort the diffraction pattern, resulting in broad fuzzy lines as seen in the left panel of Fig. 2. RHEED was also used to confirm that the growth of Fe_xMn_{1-x} films remained epitaxial and in the bcc phase up to x=0.65 with an in-plane lattice constant identical to the MgO(001) surface net. Due to the lattice mismatch these films are strained bcc films and most likely tetragonally distorted. Representative RHEED images along high symmetry directions of MgO substrate for the Fe_xMn_{1-x} are shown in the center and right panel of Fig. 2. The absence of any additional RHEED features suggests that less than 10% of the film is present in an ordered secondary phase. Higher Mn concentrations (x < 0.65) showed complex RHEED patterns indicating the loss of bcc epitaxy. It should be noted that the bcc growth of Fe_xMn_{1-x} films is similar to pure Fe films deposited on MgO where the bcc Fe lattice is rotated 45° from the MgO surface net [25]. Thus the (100) direction of the MgO(001) surface coincides with (110) direction of the epitaxial bcc Fe_xMn_{1-x} lattice.

To investigate the elemental moment variation and to examine whether ultrathin films behave similarly to the bulk, X-ray absorption spectroscopy (XAS) and X-ray magnetic circular dichroism (MCD) of 20 nm Fe_xMn_{1-x} films were acquired. Both were measured in sample current configuration at Beamline 6.3.1 of the Advanced Light Source of Lawrence Berkeley National Laboratories. By comparing the integrated $L_{2,3}$-edge XAS intensities of Fe and Mn, the Mn source temperature can be correlated with the Mn flux and therefore the concentration of Mn in the films. Precise film alloy compositions could be targeted by control of the Mn flux via the Mn source temperature by using a thermocouple in direct contact with the Mn Knudsen cell crucible. Mn Source temperature was varied from 680 °C for the lowest Mn concentration films to 852 °C for the highest concentration of Mn in the Fe_xMn_{1-x} films. Fig. 3 displays the log (base 10) of the integrated Mn XAS intensity (after normalization by the integrated Fe XAS intensity) as a function of the inverse Mn source temperature for many of the FeMn samples. Due to this normalization, the reported Mn XAS intensity is now proportional to the Mn flux rate (since the Fe flux rate is constant). The straight-line is a fit using the August equation. The August equation is similar to Antoine equation which describes vapor pressure and temperature relation for pure liquids and gasses [26,27]. From the extracted parameters of the August equation and the Rutherford backscattering data, the Mn flux rate and film composition can be determined.

The evolution of the electronic structure with alloy composition was monitored by XAS which measures the element-resolved unfilled density of states above the Fermi level. Figs. 4 and 5 display representative extremes of the evolution of the peak normalized Fe L_{23}-edge XAS and Mn L_{23}-edge XAS with Mn concentration using linear polarized X-rays, respectively. The evolution is gradual and only the limiting spectra are shown for clarity. The energies are calibrated by comparison with reference powders that are measured immediately before and after all the Fe_xMn_{1-x} films. The Fe energies are calibrated using a $ZnFe_2O_4$ powder with an L_3-peak energy of 708.22 eV and the Mn energies are calibrated by comparison with a $MnTiO_3$ powder with an L_3-peak energy of 637.90 eV. The peak energy values are determined by fitting a Gaussian to the data points near the peak energy. Additionally, new fast scan capabilities at beamline 6.3.1 minimize the time between subsequent XAS scans, resulting in more reliable energy calibration values. For the lowest Mn concentrations, the small features at energies beyond the L_2-peak beginning at 651.5 eV are from Mg K-edge absorption features (1303 eV) from the underlying MgO substrate due to 2nd harmonic light passed by the X-ray monochromator.

The Fe L_3-peak energy (inset of Fig. 4) shows a small shift to higher binding energy with increasing Mn concentrations to x=0.65 (35% Mn). For x < 0.65 (above 35% Mn), where the RHEED images show a change in crystal structure, the L_3-peak energy rapidly returns to its original value. This small shift (0.18 eV overall) can be accurately determined because of this robust energy calibration procedure. The Fe XAS spectra also exhibit an increased broadening in the L_3-peak and a slight change in the branching ratio (L_3-to-L_2 peak ratio). For this reason, integrated XAS values for the entire L_{23}-edge energy region are used for composition determination.